LA-UR-17-28571
Approved for public release; distribution is unlimited.

Title: Ancho Canyon RF Collect, March 2, 2017: Final Report

Author(s): Junor, William
Layne, John Preston
Gamble, Thomas Kirk
Quintana, Bobby Arthur
Snelson-Gerlicher, Catherine Mary
Goorley, John Timothy

Intended for: Report

Issued: 2017-09-21

Ancho Canyon RF Collect, March 2, 2017: Final Report

FINAL

Bill Junor, John Layne, Tom Gamble, Bobby Quintana, Cathy Snelson-Gerlicher, Tim Goorley

Los Alamos National Laboratory September 18, 2017

Contents

List of Figures

List of Tables

Chapter 1

Executive Summary

We report the results from the March 2, 2017, Ancho Canyon RF collection. While bright electromagnetic signals were seen nearby the firing point, there were no detections of signals from the explosively-fired fuse at a collection point about 570 m distant on the East Mesa. However, "liveness" tests of the East Mesa data acquisition system and checks of the timing both suggest that the collection system was working correctly.

We examine possible reasons for the lack of detection. Principal among these is that the impulsive signal may be small compared to the radio frequency background on the East Mesa.

Chapter 2

Introduction

The feasibility of using electromagnetic (EM) and seismo-acoustic (SA) signals collaboratively to monitor nuclear weapon testing is being investigated. The facilities at Ancho Canyon offer the opportunity to simulate — at a crude level — the EM and SA signatures. The seismo-acoustic signal can be initiated by a chemical explosion.

The electromagnetic signal may be emulated by the use of an explosively-fired fuse (EFF). These devices can generate a narrow pulse, approximately 1 μs wide, by abruptly interrupting the flow of a very large current.

The EM signature of this event is known poorly though anecdotal information suggests that it should be readily observed at low radio frequencies.

We have conducted a trial radio frequency collection against the firing of an EFF. Our goals for this test collect were:

- to exercise the RF collection system,
- to develop a RF collection plan for future experiments,
- to coordinate the activities at the firing site in Ancho Canyon with the RF data collection,
- to assess the size of the electromagnetic signal from the EFF, and
- to assess the electromagnetic background against which the EFF-generated EM signals must be detected.

As a goal of future joint collects between the seismo-acoustic sensors and the radio frequency sensors is improved geolocation of events, there is a loose requirement that the SA and EM sensors be roughly co-located. The SA sensors are either in the permanent network around Los Alamos, or as part of a temporary network installed nearby on the mesas.

We chose two sites for our RF measurements: one on the East Mesa overlooking the firing point at Point 88 in Ancho Canyon, and the other at the firing point itself. The East Mesa site had a direct line-of-sight to the firing point. The RF sensors at the firing point were an "insurance" measure to make sure we saw some RF signals associated with the event, should the signals at the East Mesa be too weak for detection.

Chapter 3

Technical approach

The pulse width is estimated to be $\approx 1\,\mu$s. Thus, the anticipated spectrum is expected to be centered around 1 MHz. Of course, the rise and fall times of the pulse are much faster so there could be additional electromagnetic information available at higher frequencies.

We have available a number of Rohde & Schwarz HE010 active monpole antennas (Rohde & Schwarz , 2017a) which have a frequency coverage from 20 kHz to ≈80 MHz. These are deployed vertically and so they are sensitive to vertical polarization only. Cheng Ho made available a 3-axis (x,y,z) custom variant of this antenna to give us a horizontally polarized sensor. To avoid saturation of the active circuitry and, potentially, the data acquisition systems, by strong FM broadcast stations and to avoid aliasing from the same, we inserted MiniCircuits low pass filters in each HE010 channel. These BLP-50+ filters suppress signals above 48 MHz (MiniCircuits , 2017).

On the East Mesa, we captured the signals on a National Instruments PXIe-1082 crate using two kinds of data aquisition cards — NI 5122 and NI 5154. The NI 5122 cards have 2 channels per card and a 100 MHz sample rate. The NI 5154 cards have 2 channels per card and a 1 GHz sample rate. The systems were disciplined with a NI GPS card (NI PXI 6682-H). We used a 10 ms window on the NI 5122 card and a 1 ms window on the NI 5154 card. Each window was centered on the top of the GPS minute *i.e.* we used a 50% pre-trigger.

Because we have a remote location and a direct firing control system trigger is impractical there, we required that the EFF event and data collection at both sites would happen at the top of the GPS minute. Moreover, we are required to vacate the East Mesa location during the EFF event and thus the East Mesa data acquisition system has to run autonomously. Thus, collecting at the top of each minute, when the exact firetime minute is not known ahead of time, is a good solution. In addition, the collections for the "empty" tops-of-minute allows us to characterize the RF background.

The East Mesa data acquisition systems were powered from two APC UPS systems. Each of these systems would allow the data acquisition to run for at least 4 hours continuously. Using UPS systems allows us to avoid impulsive ignition noise from gasoline-powered generators. (However, UPS systems do have inverters to change the power from ≈ 12 VDC to 110 VAC. Potentially, these could be a source of noise.)

The time-of-flight from the firing point to the East Mesa antennas is about 2 μs.

At the firing point location in Ancho Canyon, we deployed 3 discone antennas and a Rohde & Schwarz HE010 active monopole. Our intention here was to capture some RF signal even if the East Mesa collects were unsuccessful.

We used the LLNL data acquisition system at the firing point bunker because it was available and was integrated into the firing point control system. Each channel of the 300 MHz data acquisition rack has a 12-bit depth. The 1 GHz data acquisition system has only an 8-bit depth.

Since we did not anticipate much signal above 100 MHz, we opted for the use of the 12-bit system.

3.1 Far-field and near-field

The far-field region is where electromagnetic radiation propagates away from the source, without any back-interaction. The fields in this region are dipole-like. The far-field electromagnetic radiation field strengths fall off as 1/r. By contrast, the near-field region is governed by multipole fields which do not radiate. In this region, the phase relationship between the E and B fields is complex. See, for example, OSHA (1990)).

The transition between near-field and far-field is vaguely defined. For electromagnetically short radiators — such as we have at the EFF — the near-field is the region within a wavelength *i.e.* $r << \lambda$.

Since one component of the electromagnetic signature is expected at $\approx$ 1 MHz, the near-field region will be inside ≈30–50 m. The far-field region is typically defined to be $r >> 2\lambda$. Thus, the discones at the firing point are well within the near-field, while the nearby Rohde & Schwarz HE010 would be outside of that region, in the transitional zone. The East Mesa location is just at the inner edge of the far-field.

3.2 Anticipated signal strengths

We were advised that a similar experiment had seen electric field strengths of between 80 mV/m and 2 V/m close to the firing point. These data are unavailable to us and so we could not verify this information.

The explosively-fired fuse (EFF) has a fairly simple geometry (Figure 3.1). If we model this as an electrically-small loop in free space, then we can predict the field strength.

The electric field in the ϕ plane, E_ϕ, is

$$E_\phi = \frac{120\pi^2[I]\sin\theta A}{r\lambda^2} \tag{3.1}$$

where $[I]$ is the retarded current, A is the area of the current loop, λ is the wavelength and r is the distance from the loop (Kraus & Marhefka , 2002; Balanis , 2005). The loop is small so we can assume that the current is the same everywhere in the loop.

The line-of-sight distance from the firing point to the East Mesa data collection systems is $\approx$ 600 m. If we adopt ν = 1 MHz as the frequency of interest, *i.e.* λ = 300 m, then the collection point is just at the near-field/far-field transition. Using the geometry in

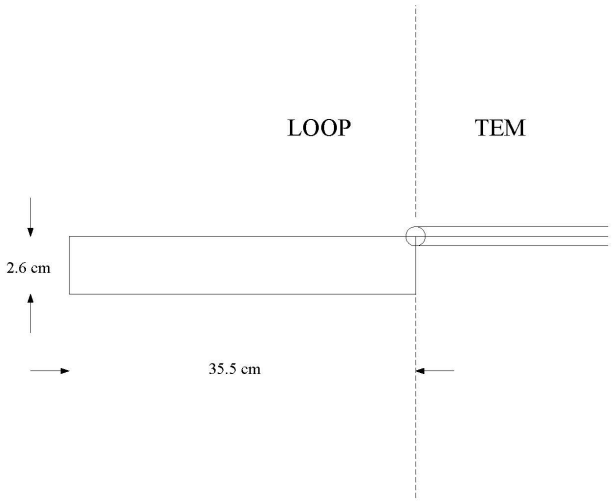

Figure 3.1: Geometry of EFF loop.

Figure 3.1 and assuming $\approx 500\,\mathrm{kA}$ in the loop, then we predict

$$E_\phi \approx 0.1\mathrm{V/m} \tag{3.2}$$

at the East Mesa collection point.

The E_ϕ field has a $\sin\theta$ dependency *i.e.* the null is along the normal to the loop. The loop normal is at about 13° to the collection point on the East Mesa. Thus, we will suffer a further attenuation of ≈ 0.23 *i.e.*

$$E_\phi \approx 0.023\mathrm{V/m}. \tag{3.3}$$

Of course, the EFF is not located in free space and the EFF is surrounded by multiple reflectors so the signal may be different from this value.

The HE010 antennas have an Antenna Factor of $17\,\mathrm{dB(1/m)}$. The antennas convert the field into voltage with

$$V[dB\,V] = E[dB\,V/m] - AF[dB\,(1/m)]. \tag{3.4}$$

Thus the anticipated voltage produced by the antennas is $\approx -49.8\,\mathrm{dBV}$ or $\approx 3.2\,\mathrm{mV}$.

The NI 5122 digitizer cards are 14-bit deep. Thus, on the 0.2 V setting, the voltage resolution is $\approx 12\,\mu\mathrm{V}$. Typically, a 14-bit ADC will have only 12 effective bit so the card's noise floor will be $\approx 50\,\mu\mathrm{V}$. This calculation indicates that the data acquisition has sufficient voltage resolution to detect the signal.

3.3 Data acquisition system at Ancho Canyon

We used 3 Centerfire "Deluxe Discone" antennas (Centerfire , 2017) close to the shot table. These have a broad frequency coverage and are cheap ($39.95). Our concern was that the close-in antennas could be damaged by flying debris from the explosion. These antennas are more than adequate for the likely field strengths close to the shot table.

We deployed an Rohde & Schwarz HE010 active monopole (Rohde & Schwarz , 2017a) about 60 m away from the shot table. We felt that there was little chance of damage to this antenna. These active monopoles are powered over the coaxial cable by a remote power supply (IN115 (Rohde & Schwarz , 2017b)). In this particular case, the power supply was located behind a blast wall on the concrete apron beside the shot table. The power supply was energized with 110 VAC supplied through an isolation transformer provided by Ancho Canyon staff. The isolation transformer is necessary to maintain a single ground point and to avoid ground loops.

The active monopole was deployed with the intention of providing another datum for the geolocation of the shot. The HE010s deployed on the East Mesa rim have very limited spatial diversity. This HE010 in the canyon would have been useful in improving the geolocation solutions.

Coaxial cables were run from all of the antennas either directly to the bunker patch panel or, in the case of the HE010 active monpole, to the power supply/bias-tee unit and then to the patch panel. Delays have been measured for all cables. These delays are $\approx 330\,\mathrm{ns}$ or less. These values have not been included here as they are not used in any

System	Antenna	Frequency coverage [GHz]	Antenna Factor [dB(1/m)]
1	Centerfire Discone	0.03–1.3	10
2	Centerfire Discone	0.03–1.3	10
3	Centerfire Discone	0.03–1.3	10
4	Rohde & Schwarz HE010	9E10-6 – 0.05	17

Table 3.1: Antenna configuration for Point 88.

analysis. The delays from the patch panel to the LLNL data acquisition system in the bunker are all very close to 114 ns.

The phase centers of the antennas are unknown. Potentially, this could introduce errors of ≈ 0.5 m in geolocation but this is a minor factor when compared to other errors in the analysis. The antennas were mounted on masts and the antenna bases were about 3 m above the ground. The positions of the antennas and the position of the firing table on which the EFF was placed were measured using a Topcon GRS-1 GPS receiver (Topcon , 2017) (Table 3.2).

3.4 Firing Point locations

System	Latitude	Longitude	Altitude [m]	Note
1	35° 48′ 30.1243″	-106° 16′ 8.2009″	1957.575	Antenna up 3m
2	35° 48′ 30.3320″	-106° 16′ 8.2122″	1957.413	Antenna up 3m
3	35° 48′ 30.2536″	-106° 16′ 7.3598″	1957.083	Antenna up 3m
4	35° 48′ 30.3611″	-106° 16′ 5.6460″	1957.254	Antenna up 3m
ST	35° 48′ 30.6090″	-106° 16′ 8.1493″	2018.709	Shot table

Table 3.2: Antenna and shot table locations at Ancho Canyon Point 88. A WGS84 datum has been used.

Figures 3.2, 3.3 and 3.4 show the set-up close to the actual firing point. Two other antennas — another discone and a Rohde & Schwarz HE010 are located further away from the firing point, down the canyon.

3.5 Liveness testing

We used a portable "pulser" system to tests the liveness of the data collection system. This pulser puts out three narrow pulses in 2 μs at specified times. The pulse schedule can be either once per minute, once every 10 seconds, or once per second. The schedule is disciplined by an integral GPS receiver.

Figure 3.5 shows the time series collected on one of the discones at the firing point. The 3 short pulses are not as distinct as they are in a similar collect on the East Mesa (Figure 3.6). We attribute this to the multiplicity of close-in reflections at the firing point.

Figure 3.2: This is the view from the firing table to discones #1 (nearer) and #2 at Point 88. The partially-assembled EFF is on the small wooden table in the foreground. (Picture from Tim Goorley.)

Figure 3.3: This is the view from discone #1 towards the firing point at Point 88. The partially-assembled EFF is at the edge of the pickup tailgate. (Picture from Tim Goorley.)

Figure 3.4: The assembled EFF on the firing table. The large metal strip in the foreground is a low inductance connection to the single ground point (out of picture). (Picture from Tim Goorley.)

3.6 Data acquisition system on East Mesa

We deployed 5 Rohde & Schwarz HE010 antennas along the rim of the East Mesa. The positions are given in Table 3.4.

In addition, we deployed a pair of Aaronia 20100e BiCoLogs (Aaronia , 2014) in a horizontal and vertical polarization configuration close to the data acquisition chassis. The positions of these antennas were not measured. The antennas were deployed to assess if there were any signals above 100 MHz from the Ancho Canyon shot.

The cable delays for all cables from the antennas to the data acquisition system were measured. These are ≈120 ns or less. However, we do not use these values in our later analysis.

System	Antenna	Frequency coverage [GHz]	Antenna Factor [dB(1/m)]	Note
1	Rohde & Schwarz HE010	9E10-6 – 0.05	17	LPF inserted
2	Rohde & Schwarz HE010	9E10-6 – 0.05	17	LPF inserted
3	Rohde & Schwarz HE010	9E10-6 – 0.05	17	LPF inserted
4	Rohde & Schwarz HE010	9E10-6 – 0.05	17	LPF inserted
5	Rohde & Schwarz HE010	9E10-6 – 0.05	17	LPF inserted
6	Rohde & Schwarz HE010	9E10-6 – 0.05	17	LPF inserted H (X axis)
7	Rohde & Schwarz HE010	9E10-6 – 0.05	17	LPF inserted V (Z axis)
8	Aaronia BiCoLog 20100e	0.02 – 1	17–34	H pol
9	Aaronia BiCoLog 20100e	0.02 – 1	17–34	V pol

Table 3.3: Antenna configuration for East Mesa.

3.7 East Mesa locations

System	Latitude	Longitude	Altitude [m]	Note
1	35° 48′ 27.2830″	-106° 15′ 44.1872″	2018.709	
2	35° 48′ 27.4732″	-106° 15′ 44.6913″	2019.752	
3	35° 48′ 27.6631″	-106° 15′ 44.9063″	2018.875	
4	35° 48′ 27.8426″	-106° 15′ 45.2493″	2018.709	
5	35° 48′ 27.2740″	-106° 15′ 45.6795″	2018.709	
6	35° 48′ 27.8361″	-106° 15′ 44.8006″	2024.341	3-axis antenna
7	35° 48′ 27.8361″	-106° 15′ 44.8006″	2024.341	3-axis antenna

Table 3.4: Low frequency antenna locations on East Mesa. We used a WGS84 datum. The positions of the Aaronia BiCoLog antennas were not measured.

3.8 Testing

We verified that our East Mesa data acquisition systen was working correctly by using our portable pulser. See Figure 3.6.

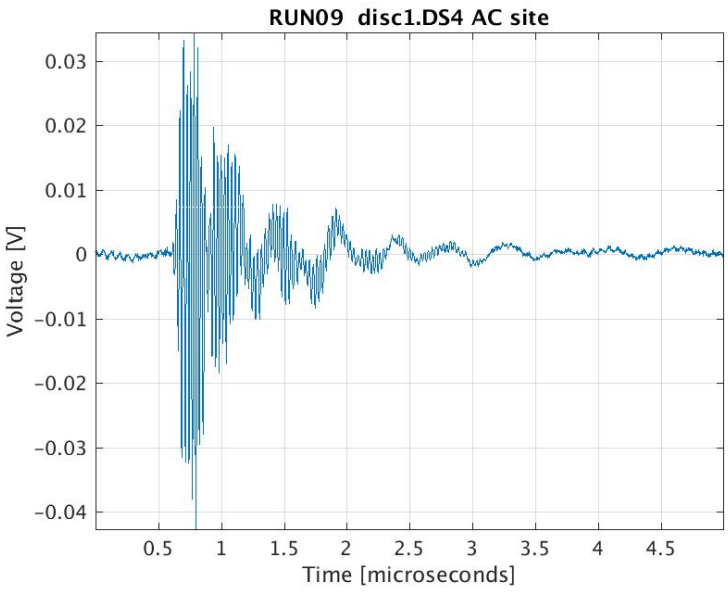

Figure 3.5: Time series for liveness test with portable pulser using discone #1 collected at Point 88.

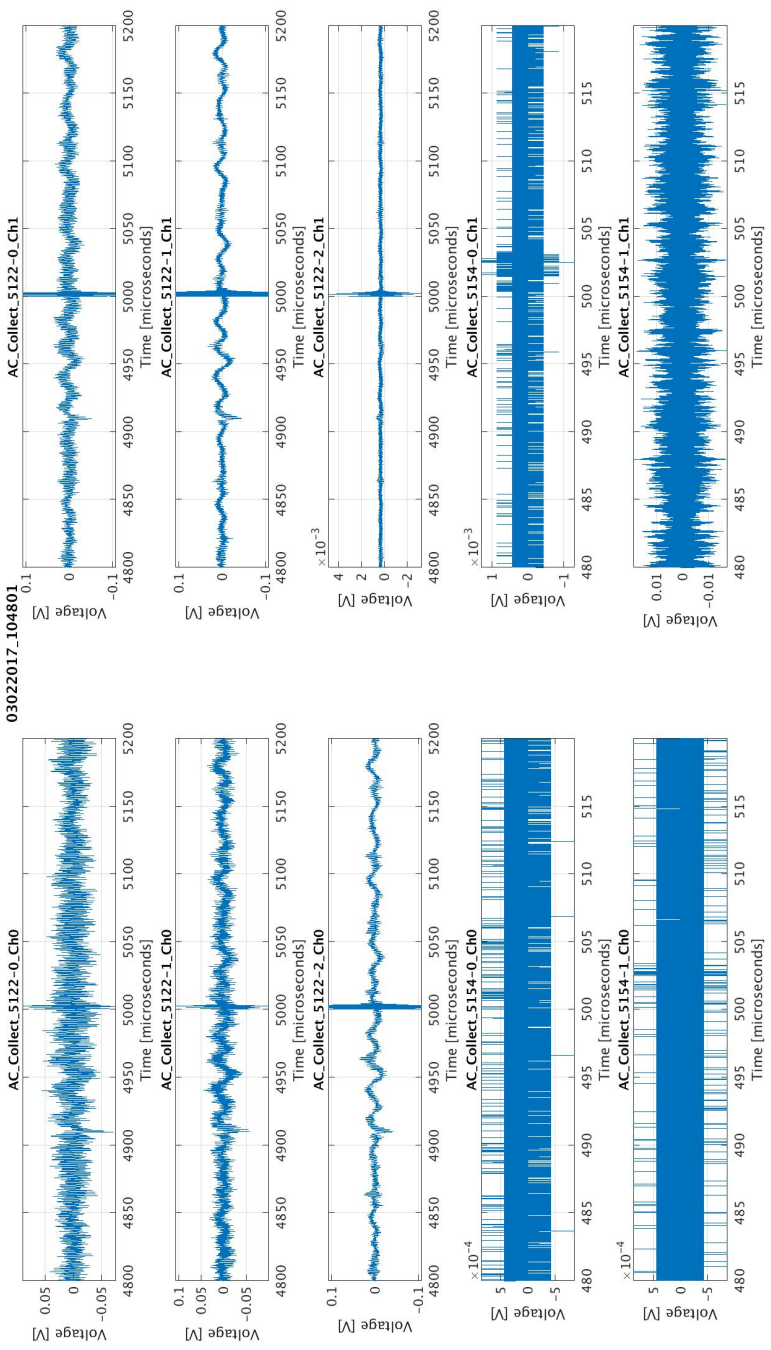

Figure 3.6: Liveness test of East Mesa data acquisition system. The pulser output is limited to a few 10s of MHz. Consequently, only the Rohde & Schwarz antennas (<50 MHz) will see any signals. The pulses are located close to 5 ms for the NI 5122 cards and 0.5 ms for the NI 5154 cards, *i.e.* close to the top of the GPS minute.

Chapter 4

Analysis

4.1 Timing chain

In Figure 4.1, we show the timing of events in the arming and firing chain.

4.2 Close to firing point

The data acquisition systems used for our four antennas were saturated with the electromagnetic signals due to the shot event (Figures 4.2, 4.3, 4.4, 4.5).

We clearly see the capacitor bank discharge, followed by an electromagnetic signature at the time of peak dI/dt at 30 μs. These times are with respect to a zero which is 10 μs after the top of the GPS minute. (See Figure 4.1.)

4.3 On East Mesa

An example of the raw collects from the East Mesa is shown in Figure 4.6. There is clearly a lot of noise, including a bright impulse at about 1600 μs into the record. The time axis gives the time from the start of the data acquisition on the NI card. The collect is centered on the top of the GPS minute so there are 5 ms of pre-trigger for the NI 5122 systems (sampling the Rohde & Schwarz HE010 antennas) and 0.5 ms pre-trigger for the NI 5154 cards. In other words, the top of the GPS minute occurs at 5000 μs and 500 μs respectively.

Figure 4.7 shows the spectrogram of that bright event in one of the NI 5122 channels. The event is located at about 1580 μs. Clearly, there are many CW carriers (horizontal lines running across the plot) and many weak impulsive events (faint vertical bars). In addition, the bulk of the power in the spectrogram is in first few MHz (*i.e.* the bright horizontal band below 2 MHz.

The data from the East Mesa collection stations have been filtered with an IIR high pass filter to remove the strong signals below 2500 kHz. (A variety of filters were applied to the data to try to extract any useful shot signals.) Figure 4.8 shows the spectrogram of the filtered data.

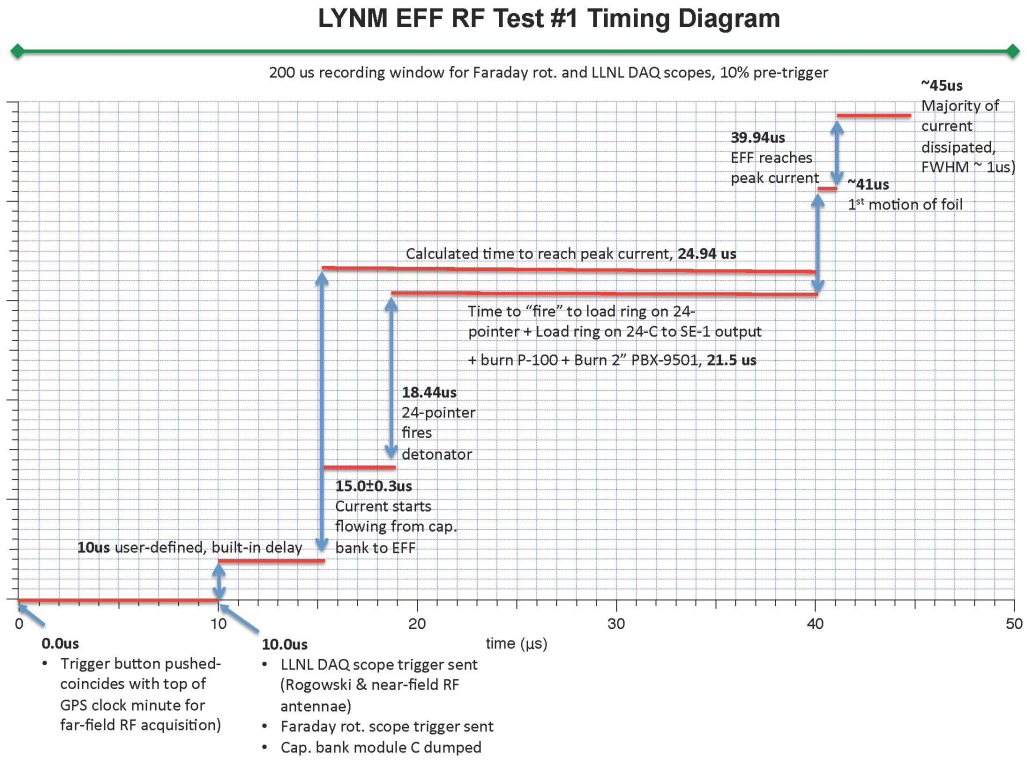

Figure 4.1: Timing diagram for the March 2, 2017, EFF shot. The peak dI/dt occurs about 40 μs after the top on the GPS minute. (Diagram supplied by Erik Haroz.)

4.4 EFF shot event

The Ancho Canyon test shot occurred at 1309 local time. At the East Mesa collection stations, we would expect any signal due to the EFF to appear at about 42 μs after the top of the GPS minute *i.e.* after $\approx$40 μs for the peak dI/dt plus $\approx$2 μs of light-travel time. In fact, we see no signals at this expected time. For example, Figure 4.9 is representative of the signals seen at the expected time.

Figure 4.10 shows all the East Mesa time series data for all channels in a window arond the expected EFF signal arrival time.

We do see strong impulsive signals in the whole collection window (10 ms straddling the top of the GPS minute) but these are unrelated to the Ancho Canyon shot.

Digging deeper into the spectrogram plots, we see faint impulsive events, possibly related to the EFF detonation firing sequence, as in Figure 4.11. There are 3 events — at 5005, 5010, 5021 and 5038μs *i.e.* at 5, 10, 21 and 38 μs after the top of the GPS minute. However, if the timing at the East Mesa and the firing point bunker are truly both slaved

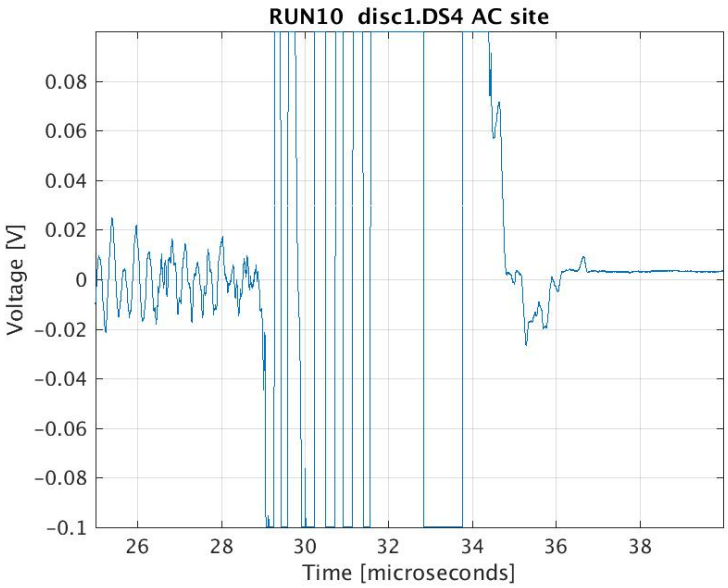

Figure 4.2: Time series for discone #1 collected at shot event.

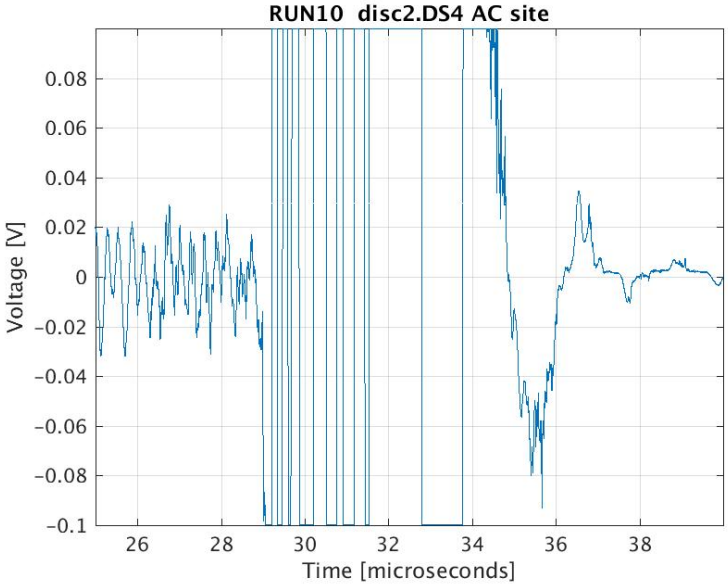

p

Figure 4.3: Time series for discone #2 collected at shot event.

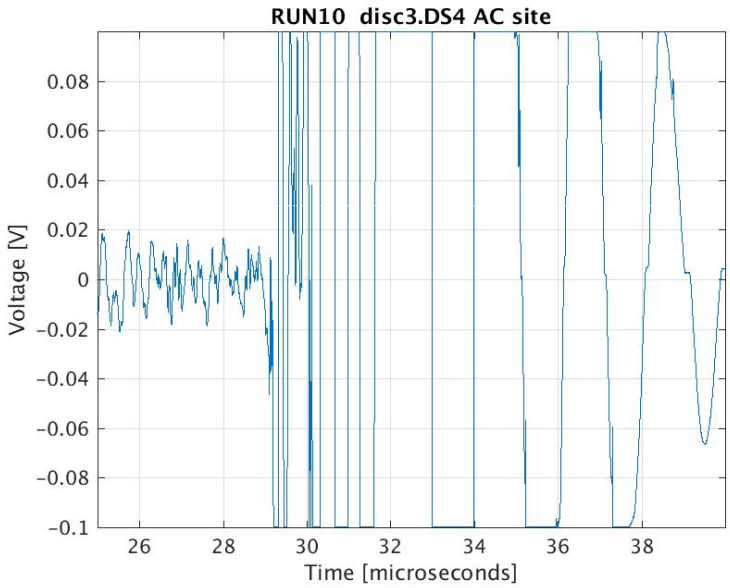

Figure 4.4: Time series for discone #3 collected at shot event.

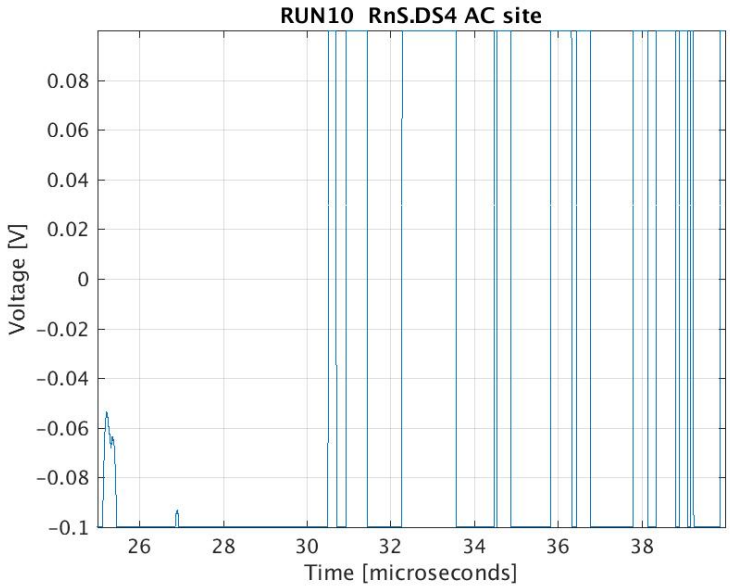

Figure 4.5: Time series for Rohde and Schwarz antenna collected at shot event.

to GPS time, then it seems hard to relate these to particular events in the timing diagram (Figure 4.1), especially when we consider the time-of-flight from the firing point to the East Mesa. Moreover, the brightest event of this series (at 5 mus) seems unrelated to anything in the timing chain.

We note also that there are many such weak, impulsive events in any of the collection window. Consequently, if these *are* related to the EFF event, then they are not detected unambiguously. The train of plausible signals in the event window also seems to be part of a larger train of repetitive signals and thus suggests that these signals are unrelated to the EFF event. (The on-screen transfer function is more useful than that of the printed page.)

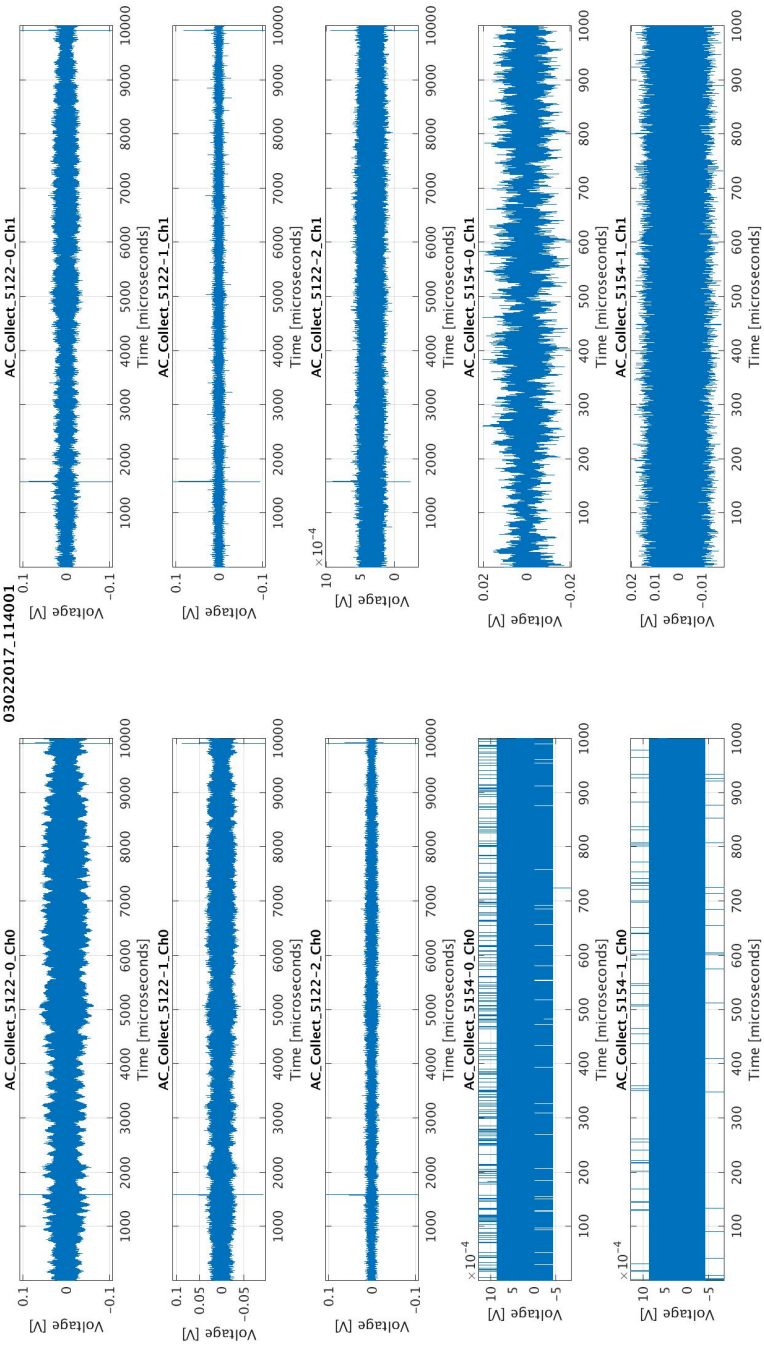

Figure 4.6: All time series collected on the East Mesa at 114001 on March 2, 2017. The top 6 panes are time series data from the NI 5122 cards. The bottom 4 panes are data from the NI 5154 cards. The NI 5122 cards had Rohde & Schwarz antennas ($< 50\,\mathrm{MHz}$) connected to their inputs. The Aaronia BiCoLog V and H pair were connected to one of 5154 cards (bottom 2 panes). One axis of the Rohde & Schwarz tri-axis antenna was connected to one input of the other NI 5154 card (fourth row, right hand side). The other NI 5154 channel was unused.

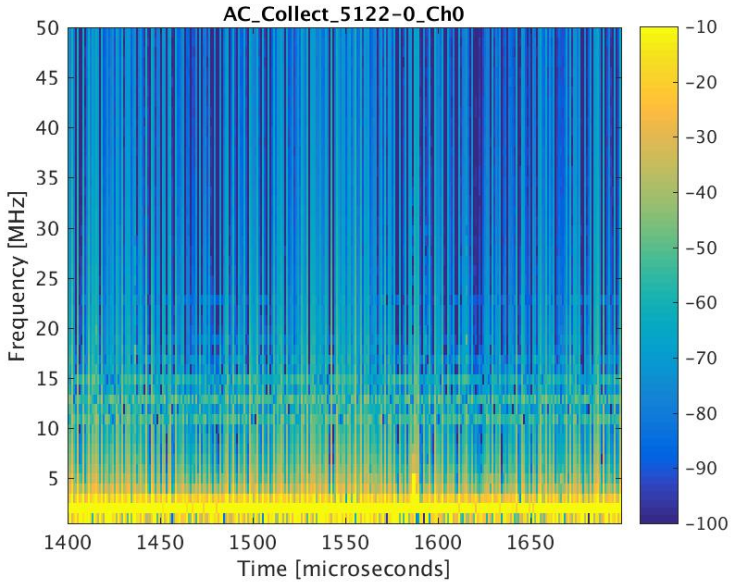

Figure 4.7: A spectrogram of a subset of the data collected from one Rohde & Schwarz HE010 on the East Mesa at 114001 on March 2, 2017.

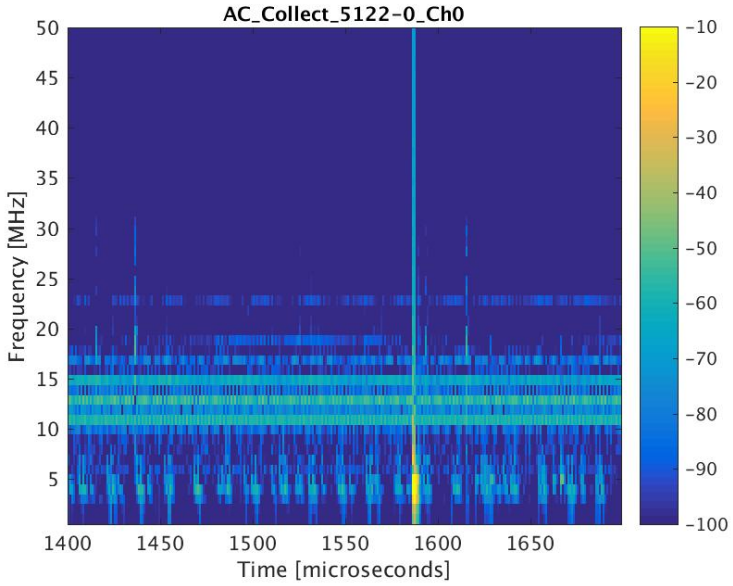

Figure 4.8: A spectrogram of a subset of the data collected from one Rohde & Schwarz HE010 on the East Mesa at 114001 on March 2, 2017, after high pass filtering.

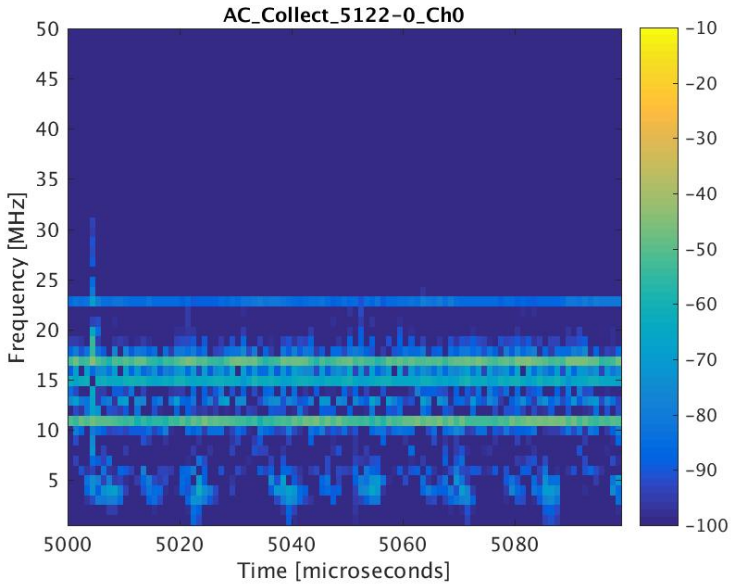

Figure 4.9: Representative spectrogram from high-pass-filtered subset of East Mesa data around the expected arrival time of the EFF signal. We expect to see an EFF-caused pulse at about 5042 μs *i.e.* 42 μs after the top of the GPS minute at 5000 μs.

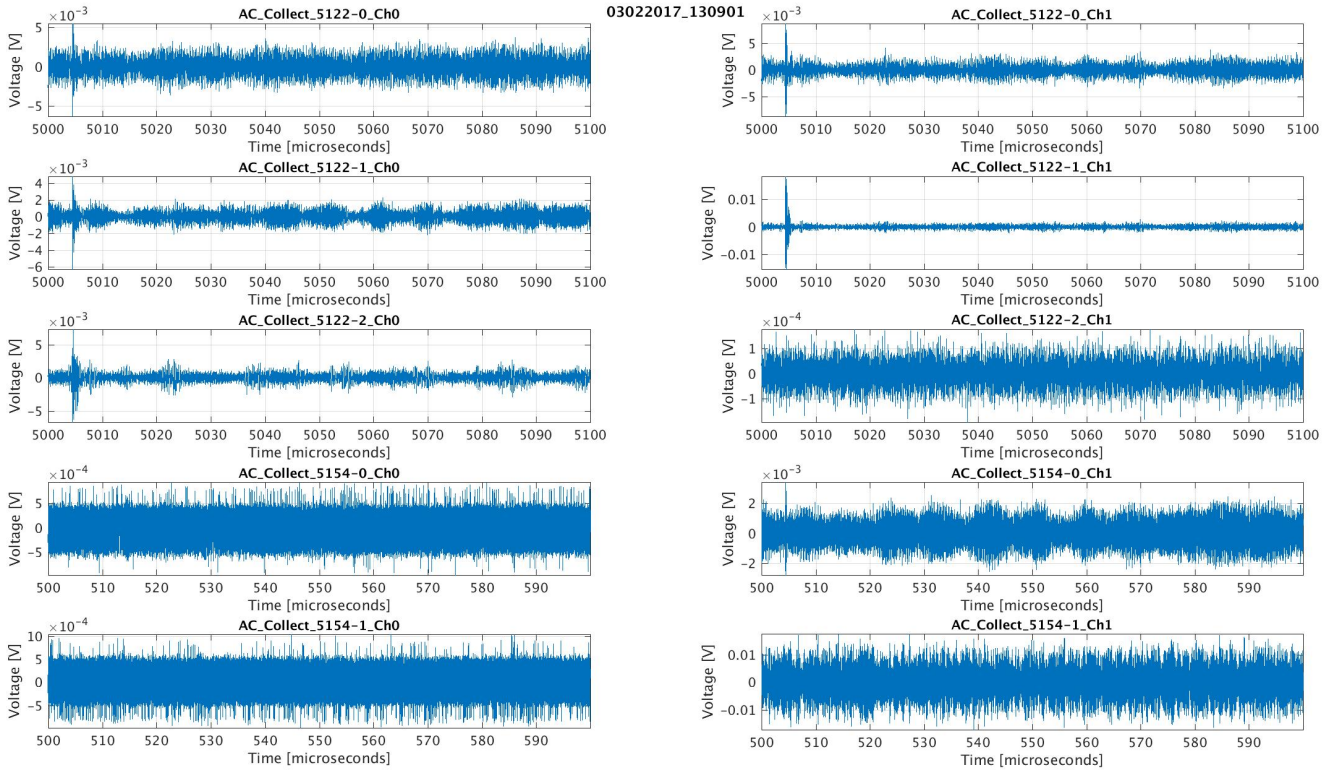

Figure 4.10: Time series near the expected arrival time for all antennas at East Mesa collection site at shot time.

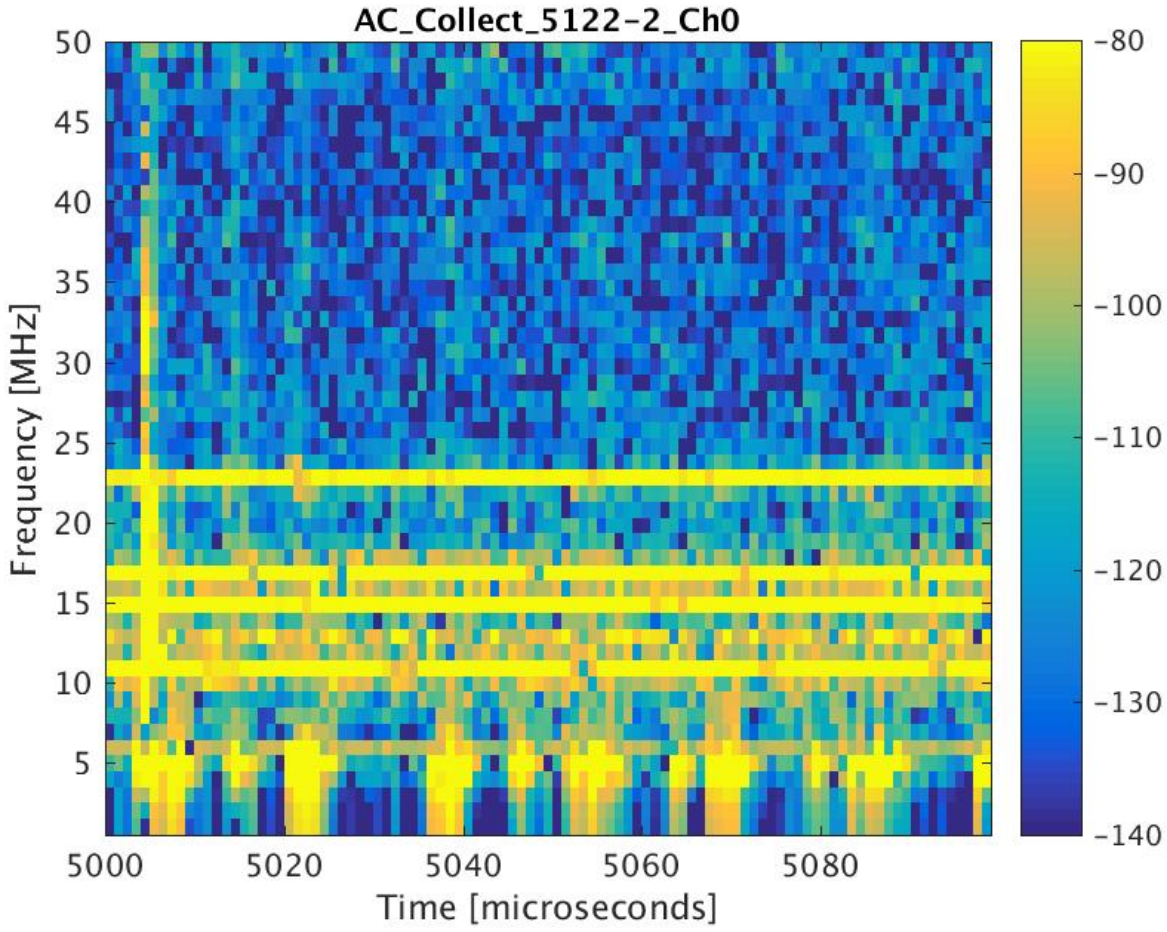

Figure 4.11: Weak impulsive events as seen on one channel of the East Mesa collects in the presumed timing window for the EFF event.

4.5 Discussion

The average r.m.s. noise over all the East Mesa HE010 active antennas channels at the time of the EFF event is about 0.63 mV (after high pass filtering). The EFF signals, if present, must be weaker than this at the East Mesa.

The ambient noise floor on the East Mesa is stronger than the signal predicted from the simple small-loop-in-free-space model.

Goforth (2017) estimates that the peak current during the EFF shot was 433 kA. This agrees with the Ancho Canyon prediction of 420 kA. Figure 4.12 shows the current profile and peak current as estimated from the integration of the Rogowski coil output. The peak current is 13% smaller than the value used in our estimate of the likely signal on the East Mesa (Section 3.2). This small difference cannot be the reason for non-detection of EFF-related signals on the East Mesa.

If we assume that the HE010 close to the firing point sees about 0.5 V at $\approx$ 50 m stand-off distance from the shot table, then we would expect to see about 44 mV at a similar antenna on the East Mesa, some 570 m from the firing point. Since this signal would be stronger than the East Mesa noise floor and since we do not see such a signal, then we conclude that the Rohde & Schwarz HE010 close to the firing point is primarily the (non-radiative) near-field primarily.

We have used the nominal Antenna Factor of 17 dB(1/m) for the Rohde & Schwarz HE010 antennas in our estimates. We note, however, that this value is for the antenna mounted on a flat, conducting plate. Our mounting configuration is different.

We have looked through the adjacent records (other top-of-minute collects) in case of a time-stamping error at the firing point bunker. Our notes from the collect indicate that the shot occurred at 1309 local time. We see no evidence of the EFF event in the adjacent records.

The possible reasons for non-detection on the East Mesa include:

- The radiated signals are below the ambient noise floor.
- The East Mesa antennas are in a radiation pattern null.
- The East Mesa antennas' polarization is orthogonal to the radiated signal from the EFF.
- There is a relative timing error between the East Mesa data acquisition and the firing point bunker data acquisition system.
- Related to the previous suggestion, our pulser check at the firing point may have given us false confidence because the conditions under which that test was made were not the same as those when the EFF shot was fired.
- Some combination of all, or most, of the above.

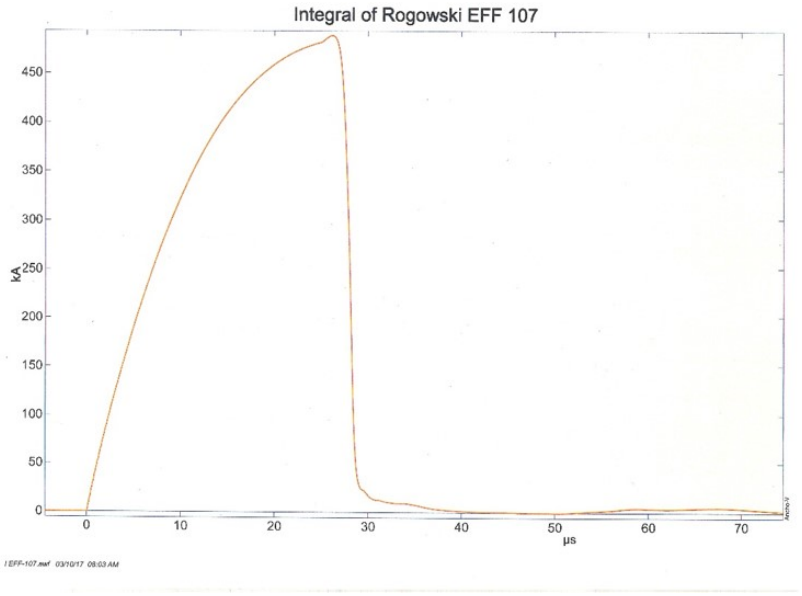

Figure 4.12: EFF current profile as inferred from Rogowski coil signal. Taken from Goforth (2017).

Chapter 5

Revision history

5.1 Revisions

- March 29, 2017: v.1.0: Initial version.
- March 30, 2017: v.1.1: Fixed LaTeX errors.
- April 3, 2017: v.1.2: Rationalized figures. Added EFF event discussion. Added discussion of use of portable pulser.
- April 4, 2017: v.1.3: Added pulser graphics. Add firing point pictures. Rotated multi-pane plots now fill one page.
- April 5, 2017: v.1.4: Added reference to Jim Goforth's interim report, deeper plotting of possible EFF-related signals.
- April 6, 2017: v.1.5: Fixed assorted typos, corrected mangled OSHA reference. Updated R&S HE010 reference.
- June 27, 2017: v.1.6: Revised AF estimate for Centerfire discones.
- August 14, 2017: v.1.7: Minor tweaks prior to submission for LA-UR.
- September 11, 2017: v.1.8: Removed "Official Use Only" from footer since this document is unclassified and uncontrolled. Fixed a few minor typos.
- September 18, 2017: v.1.9: Minor typos fixed.

Bibliography

Aaronia 20100e, 2014,
http://www.aaronia.com/products/antennas/BicoLOG-20100E-EMC-Antenna/,
accessed July 8, 2014

Balanis, C. A. 2005,
"Antenna Theory: Analysis and Design",
John Wiley & Sons, Hoboken, NJ, p.242

Centerfire Antennas, 2017,
http://centerfireantenna.com/antenna-menu/deluxe-discone-antenna/
accessed January 26, 2017

Goforth, J. 2017,
"EFF 107 Pulsed Power Results",
LANL internal project report, March 9, 2017

Kraus, J.D. and Marhefka, R.J. 2002,
"Antennas for all applications", McGraw-Hill, p.197

MiniCircuits (2017),
https://www.minicircuits.com/pdfs/BLP-50+.pdf,
accessed March 29, 2017

OSHA: Occupational Safety and Health Administration, United States Department of Labor, 1990,
https://www.osha.gov/SLTC/radiofrequencyradiation/electromagnetic_fieldmemo/elecEtromagnetic.html,
accessed April 4, 2017

Rohde & Schwarz HE010 2017,
https://www.rohde-schwarz.com/us/product/he010-productstartpage_63493-9361.html,
accessed April 6, 2017

Rohde & Schwarz IN115 2017,
https://www.rohde-schwarz.com/us/product/in115-productstartpage_63493-9363.html,
accessed March 29, 2017

Topcon 2017,
`https://www.topconpositioning.com/`,
accessed March 29, 2017